ACS Photonics

Article

pubs.acs.org/journal/apchd5

Light Emission near a Gradient Metasurface

Leonard C. Kogos and Roberto Paiella*

Department of Electrical and Computer Engineering and Photonics Center, Boston University, Boston, Massachusetts 02215, United States

Supporting Information

ABSTRACT: Gradient metasurfaces have recently emerged as a powerful tool for the control of externally incident optical wavefronts. Here we present a theoretical study showing how they can also dramatically modify the radiation properties of light emitters located in their near-field zone. First, the spontaneous emission decay of a dipole source can be greatly accelerated through near-field interactions involving evanescent waves at the metasurface, by an amount that depends on the dipole lateral position in an oscillatory fashion. Second, as a result of these interactions, highly asymmetric directional radiation patterns can be produced in the far field, with broad geometrical tunability of the angle of peak emission. Furthermore, the total output radiation power can be increased in the case of low-efficiency emitters or quenched in favor of directional excitation of surface waves depending on the metasurface phase gradient. These phenomena could not be explained simply in terms of anomalous reflection of externally incident dipole radiation by the metasurface, but rather are a direct consequence of a distinctive coupling between a wide range of evanescent and propagating waves enabled by these nanostructures. The resulting ability to control the output of radiation processes directly at the source level (without any external optics) is attractive for future applications in highly miniaturized optical systems.

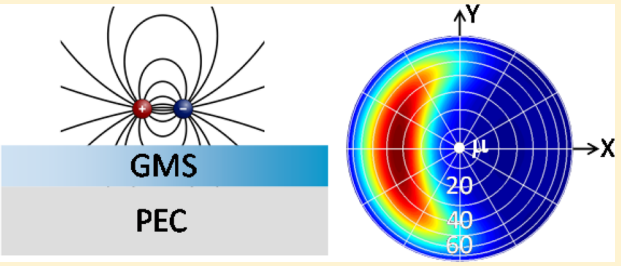

KEYWORDS: *metamaterials, surface-enhanced light emission, optical nanoantennas, surface waves*

It is well established that spontaneous emission of light is not an intrinsic process that depends only on the properties of the radiating species. Instead, the radiative decay rate is also influenced by the density of available photonic modes, which in turn is determined by the surrounding dielectric environment. The study of these phenomena dates back to Purcell's pioneering work[1] with radio waves in 1946. In photonics, the control of spontaneous emission via modifications of the local density of modes was demonstrated first in the context of fluorescence near a planar surface.[2−4] Subsequently, the same ideas have been explored with optical emitters embedded within three-dimensional artificial structures of increasing complexity (from microcavities[5] to photonic crystals[6,7] to hyperbolic metamaterials[8]) or coupled to individual metallic nanoparticles.[9] At the same time, the study of light emission near a surface has continued to receive strong interest in the field of plasmonics, with planar or nanostructured metal films used to enhance the decay rate of adjacent emitters via the near-field excitation of surface plasmon polaritons.[10−18]

Here we show that remarkable effects in this context can be obtained with a fundamentally different type of optical surface, generally referred to as a gradient metasurface (GMS), which has recently emerged from extensive research in nanophotonics.[19−29] Its basic geometry consists of a planar array of optical nanoantennas with subwavelength separation and spatially varying size, shape, and/or orientation, designed to introduce a linearly graded phase shift in the light reflected from and/or transmitted through the array. In recent years, GMSs have been used to demonstrate several notable functionalities, including anomalous reflection and refraction,[19−22] light focusing in ultrathin lenses,[23] generation of optical vortices,[19,24,27] asymmetric waveguiding,[25] and the photonic spin Hall effect.[26] In all of these works, the surface was illuminated with externally incident light having preselected wavevector and polarization. However, the unique properties of GMSs (including their ability to couple a wide range of propagating waves to surface waves[21]) also appear to be ideally suited to the near-field control of radiation processes.

In the present work, this idea is explored theoretically and then substantiated with rigorous full-wave simulations. To describe the most general possible situation, we consider the homogenized continuum model[21] shown in Figure 1a, which can be applied to any (reflective) GMS, regardless of the detailed implementation of the nanoantenna array. The light source is provided by a simple electric dipole, as appropriate to the description of spontaneous emission in typical luminescent media. Our results show that the dipole radiation output is dramatically affected by the nearby GMS, in several important and unusual ways. First, the spontaneous decay rate can be strongly enhanced through near-field interactions, by an amount that depends on the dipole lateral position in an oscillatory fashion. Second, highly asymmetric directional radiation patterns can be produced with broad geometrical

Received: September 22, 2015
Published: January 14, 2016

DOI: 10.1021/acsphotonics.5b00544
ACS Photonics 2016, 3, 243−248

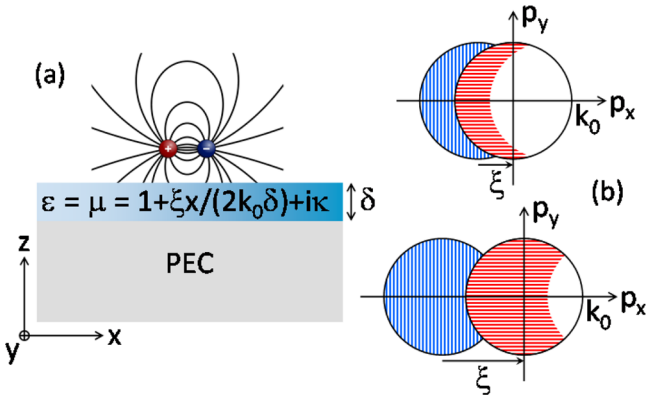

Figure 1. (a) Schematic cross-sectional view of the GMS model used in this work. (b) Distribution of the plane-wave components of the dipole field $\mathbf{E}_{dip}$ involved in the main radiation process, for $\xi/k_0 = 0.6$ (upper plot) and 1.4 (lower plot). Here $\mathbf{p}$ denotes the in-plane wavevector; the vertically dashed region is the set of all evanescent components of $\mathbf{E}_{dip}$ that can be scattered by the GMS into radiation; the resulting propagating waves are contained in the horizontally dashed region.

tunability of the angle of peak emission. Furthermore, the total output radiation power can be increased in the case of low-efficiency emitters or quenched in favor of asymmetric surface-wave excitation depending on the GMS phase gradient. These results shed new light on the distinctive properties of GMSs and underscore their potential to enable novel applications involving, for example, extremely miniaturized and high-speed light-emitting devices, photonic integrated circuits, or highly multiplexed fluorescence sensors.

RESULTS AND DISCUSSION

The model system considered in this work consists of a perfect electric conductor (PEC) coated with a metamaterial slab of highly subwavelength thickness δ and position-dependent permittivity ε and permeability μ. In this geometry, illustrated schematically in Figure 1a, the phase shift upon reflection for a normally incident harmonic plane wave is $\Phi = 2\mathrm{Re}\{\sqrt{\varepsilon\mu}\}k_0\delta$, where $k_0 = 2\pi/\lambda_0$ is the free-space wavenumber. A linear phase gradient ξ along any specific in-plane direction (e.g., the x direction) is then obtained with $\varepsilon = \mu = 1 + \xi x/(2k_0\delta) + i\kappa$,[21] which gives $\Phi = 2k_0\delta + \xi x$. The imaginary term κ in this expression accounts for the GMS absorption losses and therefore determines the normal-incidence power reflection coefficient $R = \exp(-4\mathrm{Im}\{\sqrt{\varepsilon\mu}\}k_0\delta) = \exp(-4\kappa k_0\delta)$. Because of the phase gradient $\xi\hat{\mathbf{x}}$, light incident with in-plane wavevector $\mathbf{p}$ is diffractively scattered into a reflected wave of wavevector components parallel and perpendicular to the GMS given by $\mathbf{k}_{\parallel,r} = \mathbf{p} + \xi\hat{\mathbf{x}}$ and $k_{\perp,r} = \sqrt{k_0^2 - k_{\parallel,r}^2}$, respectively. At the same time, all other diffraction orders including specular reflection are completely suppressed. If $k_{\parallel,r} < k_0$, $k_{\perp,r}$ is real and the reflected wave propagates away from the surface with a nonspecular angle of reflection $\theta_r = \mathrm{atan}(k_{\parallel,r}/k_{\perp,r})$ (anomalous reflection). Otherwise, $k_{\perp,r}$ is imaginary and a surface wave bound to the GMS is produced.

In practice, the behavior just described can be obtained with a planar array of ultrathin antennas (e.g., H- or rectangular-shaped[21,22,28]) of varying size, separated from a metal-film "ground plane" by a thin dielectric layer. Compared to designs without a metallic substrate, such reflective GMSs can provide substantially improved scattering efficiency. For instance, in ref 22 a relatively large power reflection coefficient R of 80% was measured at visible wavelengths (850 nm). Due to the discrete nature of the individual nanoantennas, the phase gradient of these arrays is essentially discretized into a staircase of roughly equal phase steps. While the model system of Figure 1a does not account for this granularity, it has already been used effectively to describe prior experimental work involving the reflection of externally incident light from GMSs.[21,25] Its applicability to the study of GMS-enhanced light emission is discussed in the Supporting Information, together with additional simulation results obtained with a specific design from the literature consisting of a discrete arrangement of patch nanoantennas.[22] The key conclusions presented below based on the homogenized continuum model of Figure 1a are confirmed by these additional simulations.

The radiative properties of a dipole near a surface such as the GMSs under study can be described using a semiclassical model of luminescence, where the spontaneous emission rate Γ_{sp} is computed from the work per unit time done by the dipole on the electromagnetic field, divided by the photon energy.[3,4] In this approach, $\Gamma_{sp} = -1/(2\hbar)\mathrm{Im}\{\boldsymbol{\mu}^*\cdot\mathbf{E}_{tot}\}$, where $\boldsymbol{\mu}$ is the dipole moment and $\mathbf{E}_{tot}$ is the total (emitted plus reflected) electric field at the dipole location. The electric field directly emitted by the dipole $\mathbf{E}_{dip}$ can be conveniently expanded in a superposition of plane waves of complex amplitudes $\mathbf{E}_{dip}(\mathbf{p})$ for all values of the in-plane wavevector $\mathbf{p}$ (including evanescent terms with $p > k_0$). At the GMS, each such wave produces a reflected wave (also possibly evanescent) of in-plane wavevector $\mathbf{p} + \xi\hat{\mathbf{x}}$ and complex amplitude $\mathbf{E}_r(\mathbf{p} + \xi\hat{\mathbf{x}}) \propto \mathbf{E}_{dip}(\mathbf{p})$. The spontaneous emission rate can then be written as

$$\Gamma_{sp} = -\frac{1}{2\hbar}\int \mathbf{dp}\ \mathrm{Im}\{\boldsymbol{\mu}^*\cdot[\mathbf{E}_{dip}(\mathbf{p}) + \mathbf{E}_r(\mathbf{p} + \xi\hat{\mathbf{x}})]\} \quad (1)$$

with $\mathbf{E}_{dip}(\mathbf{p})$ and $\mathbf{E}_r(\mathbf{p} + \xi\hat{\mathbf{x}})$ computed at the dipole location. Each term in the integral of eq 1 measures the probability per unit time that the dipole emits light with in-plane wavevector $\mathbf{p}$. This probability can be strongly enhanced by the GMS if the reflected field is large at the dipole location and has the proper phase relationship with the dipole so as to reinforce its oscillations.

With this framework, we can present the following picture of light emission near a GMS. The propagating waves $\mathbf{E}_{dip}(\mathbf{p})$ (with $p < k_0$) emitted by the dipole toward the GMS are scattered into either anomalously reflected waves or surface waves depending on the value of $\mathbf{p}$. The resulting surface waves are bound to the GMS and cannot radiate. At the same time, if the dipole distance d from the GMS is much smaller than the wavelength λ_0, they can produce a large contribution to eq 1, by virtue of the strong field confinement of evanescent waves near the surface. As a result, the dipole decay rate Γ_{sp} is enhanced. In addition, for $d \ll \lambda_0$ some of the evanescent components of $\mathbf{E}_{dip}$ can be diffracted by the GMS into propagating waves and therefore contribute to both the decay-rate enhancement and the radiation output. This process is illustrated schematically in Figure 1b for two values of the normalized phase gradient ξ/k_0 (0.6 and 1.4). In these plots, the center circle of radius k_0 is the boundary of the light cone at the dipole radiation frequency. The vertically dashed region is the set of all evanescent components of $\mathbf{E}_{dip}$ that can be diffractively scattered into radiation, and the resulting propagating waves are contained in the horizontally dashed region. Since this radiation mechanism is mediated by near-field interactions involving highly confined

DOI: 10.1021/acsphotonics.5b00544
ACS Photonics 2016, 3, 243−248

evanescent fields, it can be expected to occur with high probability and thus dominate the dipole emission. Under these conditions, the far-field radiation pattern will mostly consist of plane-wave components from within the horizontally dashed region of Figure 1b, leading to directional emission. Finally we note that, in the geometry under study, the local phase difference between any incident plane wave and its reflection varies periodically as a function of x with period $2\pi/\xi$ (i.e., the distance over which the GMS reflection phase Φ changes by 2π). Since the dipole decay rate of eq 1 depends strongly on this phase relationship, it can be expected to undergo similarly periodic variations with the dipole position along the x direction.

In order to verify and quantify these expectations, rigorous simulations based on the finite difference time domain (FDTD) method were carried out. In these simulations, the GMS is described with the homogenized continuum model presented earlier, and the light source is an oscillating dipole oriented along the x, y, or z direction (as defined in Figure 1a). All results presented below are computed at a representative visible wavelength λ_0 of 800 nm, but can be readily scaled to other wavelengths. The thickness δ of the metamaterial layer above the PEC is set to $\lambda_0/20$, and the imaginary permittivity and permeability κ is taken to be 0.18. With this choice of parameters, the power reflection coefficient $R = \exp(-4\kappa k_0\delta)$ is equal to the aforementioned value of 80% measured in ref 22 with a reflective GMS at similar visible wavelengths. Therefore, the model used in this work contains a realistic description of the GMS absorption losses. In the present context, such losses can limit the dipole radiative efficiency and cause a broadening of the radiation patterns if absorption by the GMS is stronger than diffractive scattering. The numerical simulation results presented below indicate that for $\kappa = 0.18$ these effects do not provide any significant limitation.

The color maps of Figure 2a–d show the calculated far-field radiation patterns of a dipole oriented along the z direction (i.e., perpendicular to the GMS) for different values of ξ/k_0. The dipole is located at a distance $d = \lambda_0/100$ from the surface and has lateral position $x = x_c$ (the center of the FDTD simulation region, where the reflection phase Φ happens to be $2k_0\delta$). Highly asymmetric directional emission is clearly observed, with the angle of peak intensity rotating from the negative toward the positive x direction as ξ/k_0 increases. At the same time, the angular width of the radiation pattern also increases with the phase gradient. These results are in excellent agreement with the qualitative picture presented above. The light emission appears to be dominated by the evanescent components of the dipole field that can be diffractively scattered into radiation by the GMS. As a result, the intensity distribution in the far-field pattern is mostly concentrated within the horizontally dashed region of Figure 1b, whose width along the p_x direction increases with increasing ξ/k_0. Importantly, these results could not be explained simply in terms of anomalous reflection of externally incident dipole radiation (in fact, very different patterns would be obtained in that case), which highlights the key role played by near-field interactions in the radiation process under study.

Similar results are obtained with a dipole at the same location oriented along the x direction (i.e., parallel to the GMS and to the phase gradient), as illustrated in Figure 2e for $\xi/k_0 = 0.6$. In contrast, a y-oriented dipole at this particular location is found to produce nearly opposite radiation patterns, i.e., with stronger emission within the nondashed region of the light circle of

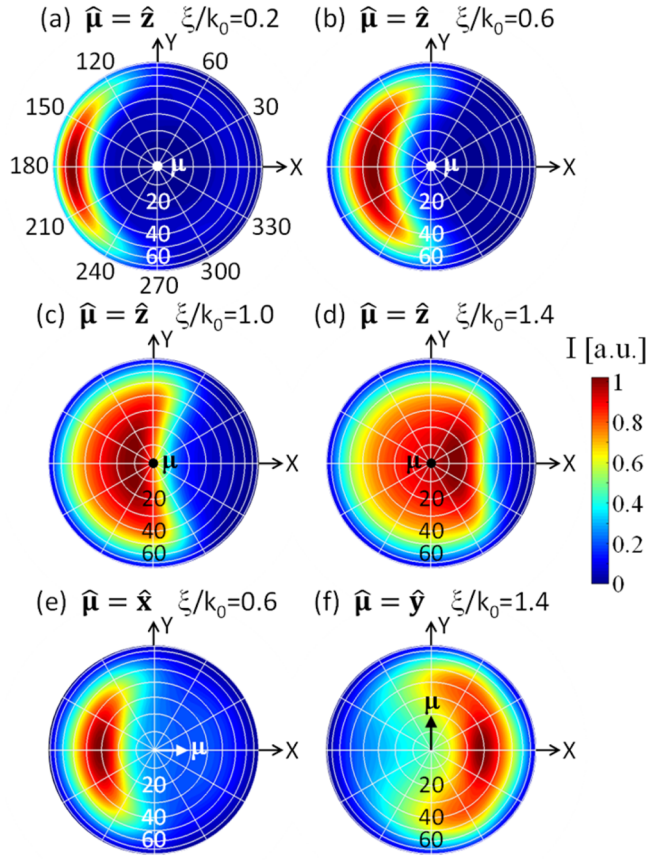

Figure 2. Far-field radiation patterns (i.e., optical intensity I versus emission angles) for $d = \lambda_0/100$, $x = x_c$, and different normalized phase gradients ξ/k_0. (a–d) Dipole oriented perpendicular to the GMS. (e) Dipole oriented parallel to the GMS phase gradient. (f) Dipole oriented parallel to the GMS but perpendicular to the phase gradient. In each plot, the radial distance from the origin corresponds to the polar angle, while the direction on the circle corresponds to the azimuthal angle. Each color map is normalized to its peak value.

Figure 1b. One example is shown in Figure 2f, for $\xi/k_0 = 1.4$. This behavior is attributed to the phase relationship between the scattered waves in the horizontally dashed region of Figure 1b and the dipole oscillations, which in the present case appears to be inadequate to produce a large increase in emission rate. As a result, these scattered waves give a weaker contribution to the light output relative to the propagating components of $\mathbf{E}_{dip}$ and their anomalous reflection.

Further insight is obtained by computing the equivalent Purcell enhancement factor of the GMS, defined as $F_P \equiv \Gamma_{sp}/\Gamma^0_{sp}$, where Γ_{sp} and Γ^0_{sp} are the dipole emission rates near the GMS and in free space, respectively. In the FDTD simulations, F_P is calculated as the ratio between the total power emitted by the dipole (into both radiative and surface waves) with and without the GMS. With this procedure, large Purcell factors of up to several 100 are obtained, indicative of strong coupling between the GMS and the emitter. For fixed GMS geometry, F_P is found to depend on the dipole position in two important ways. First, it decays rapidly with increasing distance d from the GMS on a length scale well below the free-space emission wavelength λ_0, as shown in Figure 3a for all three dipole orientations, $\xi/k_0 = 1.4$, and $x = x_c$. This behavior is consistent with the key role played by evanescent waves in the observed spontaneous-emission rate enhancement. Second, the Purcell

DOI: 10.1021/acsphotonics.5b00544
ACS Photonics 2016, 3, 243–248

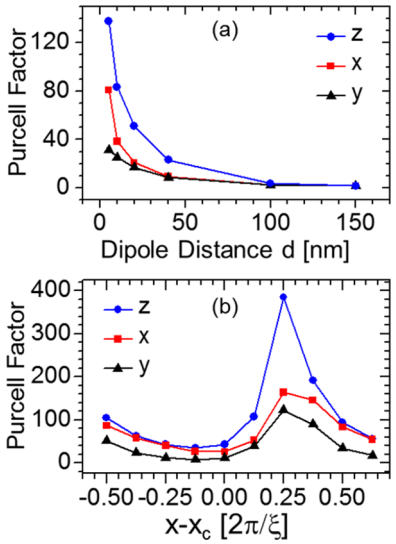

Figure 3. Purcell enhancement factor F_P for all three dipole orientations versus (a) dipole distance from the GMS and (b) dipole lateral position. The GMS normalized phase gradient ξ/k_0 is 1.4 in (a) and 0.6 in (b).

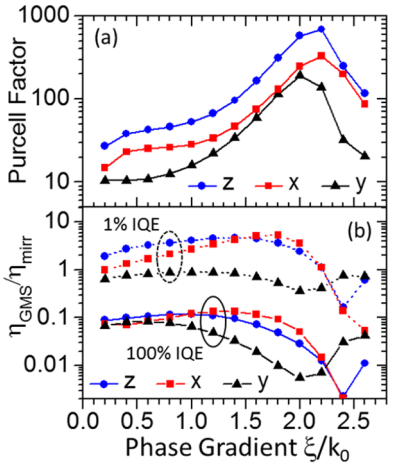

Figure 4. (a) Purcell enhancement factor F_P for $d = \lambda_0/100$, $x = x_c$, and all three dipole orientations, versus GMS phase gradient ξ/k_0. (b) Radiative efficiency ratio η_{GMS}/η_{mirr} versus ξ/k_0 for a dipole with IQE of 100% (solid traces) and 1% (dashed traces).

factor is found to vary periodically with the dipole lateral position x with period $2\pi/\xi$, as expected due to the aforementioned periodic x dependence of the phase difference between $\mathbf{E}_{dip}$ and $\mathbf{E}_r$. To illustrate, in Figure 3b F_P is plotted as a function of $x - x_c$ for $\xi/k_0 = 0.6$ and $d = \lambda_0/100$. Similar results are predicted for GMSs of different phase gradients ξ, with the lateral position of maximum Purcell enhancement depending on the specific value of ξ.

The directional and position-dependent radiation properties just described are unique in the context of surface-enhanced light emission and may be exploited to enable useful new functionalities. In practice, in the case of a continuous distribution of (isotropic) dipoles near a GMS, the light output will be dominated by the regions (and dipole orientations) of highest emission rate. Under these conditions, the radiation patterns described by the basic picture of Figure 1b are therefore obtained. On the other hand, if highly localized sources (such as single molecules or quantum dots) are employed, the GMS also allows controlling the decay rate and directionality of each emitter separately based on its location.

The Purcell factor also depends on the GMS phase gradient ξ/k_0, as shown in Figure 4a for a dipole at $d = \lambda_0/100$ and $x = x_c$. A pronounced peak in F_P is observed near $\xi/k_0 \approx 2$ for all three dipole orientations, which is again consistent with the qualitative picture above. In this picture, the decay rate enhancement is largely caused by radiative scattering of the evanescent components within the vertically dashed region of Figure 1b. Therefore, F_P increases with the area of this region, which in turn increases with ξ/k_0 for $\xi/k_0 \leq 2$ (as illustrated by the two panels of Figure 1b). When ξ/k_0 is increased beyond 2, the vertically dashed region reaches its maximum possible area (equal to that of the light circle), but moves to larger and larger values of $\mathbf{p}$. The resulting decrease in F_P is then attributed to a progressively diminishing contribution to the probability rate of eq 1 from the evanescent components of $\mathbf{E}_{dip}$ with increasing $\mathbf{p}$. A similar argument can be made regarding the ξ/k_0 dependence of the number of propagating components of $\mathbf{E}_{dip}$ scattered into surface waves, which also contribute to F_P.

Next, we consider the dipole radiative efficiency $\eta = \Gamma_{rad}/(\Gamma_{sp} + \Gamma_{nr})$, where Γ_{sp} is the aforementioned total spontaneous emission rate (into both radiative and surface waves), Γ_{rad} is the decay rate due to the emission of output radiative modes only, and Γ_{nr} accounts for nonradiative decay processes intrinsic to the emitter material. From the FDTD simulations we can determine Γ_{sp} and Γ_{rad} (normalized to Γ^0_{sp}), by computing the power through, respectively, a closed surface containing only the dipole and a planar surface located immediately above its near field. The nonradiative term $\Gamma_{nr}/\Gamma^0_{sp}$ does not enter the FDTD calculations, but can be included in the subsequent analysis as an input parameter, related to the dipole internal quantum efficiency IQE $= \Gamma^0_{sp}/(\Gamma^0_{sp} + \Gamma_{nr})$. With this procedure, described in more detail in the Supporting Information, we have computed the radiative efficiency near the reflective GMSs under study (η_{GMS}) and, for comparison, that of an identical dipole above a perfect mirror (η_{mirr}).

In Figure 4b, the ratio η_{GMS}/η_{mirr} is plotted versus ξ/k_0 for $d = \lambda_0/100$ and $x = x_c$. The solid and dashed traces correspond to a dipole source with IQE = 100% and 1%, respectively. As illustrated by these data, the GMS can either enhance or decrease the radiative efficiency, as a result of two competing effects. First, some of the dipole emission is always captured by the GMS via scattering into surface waves. Therefore, if the dipole has a large IQE to begin with, its radiative efficiency is necessarily decreased near the GMS. Second, by virtue of the large Purcell factors just described, the probability rate of spontaneous emission can be significantly enhanced by the GMS relative to that of nonradiative decay processes. As a result, in low-IQE sources the latter processes can become less of a limiting factor, leading to increased emission. As shown in Figure 4b, for IQE = 1% such Purcell enhancement effects can already overcome the optical losses in GMSs with $\xi/k_0 \leq 2$. Thus, a sizable increase in radiative efficiency (up to over 5×) is obtained, particularly for the x- and z-oriented dipoles in this case. For the y-dipoles, η_{GMS} is limited by the weaker contribution to Γ_{sp} from their evanescent components at $x = x_c$, as discussed previously, but larger values can be obtained at nearby positions. Furthermore, in practice significantly larger enhancements in the collected output power can be expected for all dipole orientations, by virtue of the increased directionality produced by the GMS.

DOI: 10.1021/acsphotonics.5b00544
ACS Photonics 2016, 3, 243−248

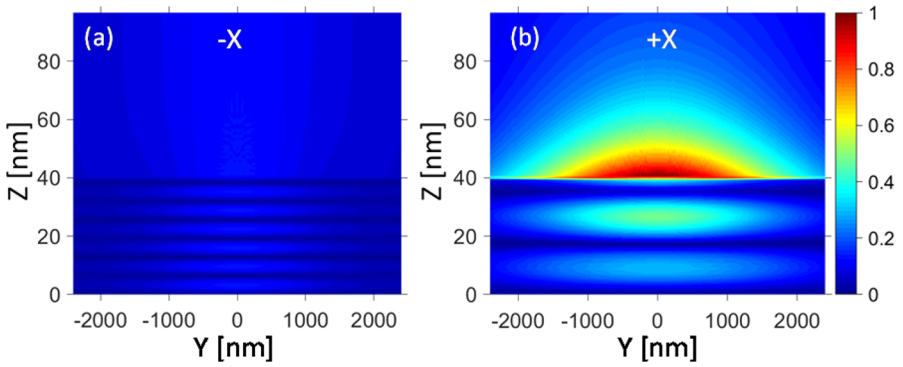

Figure 5. Optical power distribution on a monitor plane perpendicular to the x-axis near the left (a) and right (b) boundary of the FDTD simulation region, computed with a z-oriented dipole near a GMS with $\xi/k_0 = 2.6$. The color bar is the same for both plots. The GMS−air interface is at $z = 40$ nm.

Finally, for $\xi/k_0 > 2$ all downward propagating components of the dipole field are diffracted into surface modes, and the GMS-mediated light emission involves only radiative scattering of high-**p** evanescent components (with progressively diminishing Purcell factor). In this regime, the radiative efficiency is therefore mostly quenched even for low-IQE dipoles, in favor of efficient excitation of surface waves at the GMS. Importantly, the latter process is also directional, with all the excited surface waves having a positive x-component of their wavevector, as a result of the asymmetric nature of diffraction by the GMS. To illustrate, in Figure 5 we show the calculated power distribution on two planes perpendicular to the GMS, located at the same distance (∼3 μm) from the dipole along the negative and positive x direction. In both plots, the phase gradient is $\xi/k_0 = 2.6$, and the dipole is oriented along the z direction and positioned at $d = \lambda_0/100$ and $x = x_c$. A highly localized surface wave is clearly observed propagating away from the dipole along the positive x direction (Figure 5b), while significantly less power is computed on the other side (Figure 5a). It should be noted that such asymmetric excitation of surface waves from a nearby source is attractive for applications in nanoscale photonic integrated circuits.

In conclusion, we have presented general theoretical arguments supported by rigorous numerical simulations showing that GMSs provide unique opportunities for the near-field control of radiation processes, by virtue of the distinctive coupling between evanescent and propagating modes enabled by their phase gradient. Their flat ultrathin geometry is also particularly well suited to promote such near-field interactions. The resulting ability to tailor the light output directly at the source level (without the need for any bulky external optics) is technologically significant for the continued miniaturization of optical components and could be extended to other radiation mechanisms such as those involving nonlinear optical processes. More advanced beam-shaping functionalities via similar near-field interactions can also be envisioned with GMS phase profiles of increased complexity.

■ ASSOCIATED CONTENT

Supporting Information

The Supporting Information is available free of charge on the ACS Publications website at DOI: 10.1021/acsphotonics.5b00544.

Additional information on the FDTD simulation methods; detailed discussion of the applicability of the homogenized continuum model of Figure 1a to the study of GMS-enhanced light emission; additional simulation results for a specific GMS design based on a discrete arrangement of nanoantennas (PDF)

■ AUTHOR INFORMATION

Corresponding Author

*E-mail: rpaiella@bu.edu.

Notes

The authors declare no competing financial interest.

■ ACKNOWLEDGMENTS

This work was supported by the Department of Energy under Grant DE-FG02-06ER46332. The FDTD simulations were performed using the Shared Computing Cluster facility at Boston University.

■ REFERENCES

(1) Purcell, E. M. Spontaneous Emission Probabilities at Radio Frequencies. *Phys. Rev.* **1946**, *69*, 681.

(2) Drexhage, K. H. Interaction of Light with Macromolecular Dye Layers. In *Progress in Optics*; Wolf, E., Ed.; North Holland, 1974; pp 163−232.

(3) Ford, G. W.; Weber, W. H. Electromagnetic Interactions of Molecules with Metal Surfaces. *Phys. Rep.* **1984**, *113*, 195−287.

(4) Barnes, W. L. Fluorescence Near Interfaces: the Role of Photonic Mode Density. *J. Mod. Opt.* **1998**, *45*, 661−699.

(5) Gerard, J. M.; Sermage, B.; Gayral, B.; Legrand, B.; Costard, E.; Thierry-Mieg, V. Enhanced Spontaneous Emission by Quantum Boxes in a Monolithic Optical Microcavity. *Phys. Rev. Lett.* **1998**, *81*, 1110−1113.

(6) Yablonovitch, E. Inhibited Spontaneous Emission in Solid-State Physics and Electronics. *Phys. Rev. Lett.* **1987**, *58*, 2059−2062.

(7) Noda, S.; Fujita, M.; Asano, T. Spontaneous-Emission Control by Photonic Crystals and Nanocavities. *Nat. Photonics* **2007**, *1*, 449−458.

(8) Krishnamoorthy, H. N. S.; Jacob, Z.; Narimanov, E.; Kretzschmar, I.; Menon, V. M. Topological Transitions in Metamaterials. *Science* **2012**, *336*, 205−209.

(9) Novotny, L.; van Hulst, N. Antennas for Light. *Nat. Photonics* **2011**, *5*, 83−90.

(10) Amos, R. M.; Barnes, W. L. Modification of the Spontaneous Emission Rate of Eu^{3+} Ions Close to a Thin Metal Mirror. *Phys. Rev. B: Condens. Matter Mater. Phys.* **1997**, *55*, 7249−7254.

(11) Gontijo, I.; Boroditsky, M.; Yablonovitch, E.; Keller, S.; Mishra, U. K.; DenBaars, S. P. Coupling of InGaN Quantum-Well Photoluminescence to Silver Surface Plasmons. *Phys. Rev. B: Condens. Matter Mater. Phys.* **1999**, *60*, 11564−11567.

DOI: 10.1021/acsphotonics.5b00544
ACS Photonics 2016, 3, 243−248

(12) Shimizu, K. T.; Woo, W. K.; Fisher, B. R.; Eisler, H. J.; Bawendi, M. G. Surface-Enhanced Emission from Single Semiconductor Nanocrystals. *Phys. Rev. Lett.* **2002**, *89*, 117401.
(13) Okamoto, K.; Niki, I.; Shvartser, A.; Narukawa, Y.; Mukai, T.; Scherer, A. Surface-Plasmon-Enhanced Light Emitters Based on InGaN Quantum Wells. *Nat. Mater.* **2004**, *3*, 601−605.
(14) Paiella, R. Tunable Surface Plasmons in Coupled Metallo-Dielectric Multiple Layers for Light Emission Efficiency Enhancement. *Appl. Phys. Lett.* **2005**, *87*, 111104.
(15) Song, J. H.; Atay, T.; Shi, S.; Urabe, H.; Nurmikko, A. V. Large Enhancement of Fluorescence Efficiency from CdSe/ZnS Quantum Dots Induced by Resonant Coupling to Spatially Controlled Surface Plasmons. *Nano Lett.* **2005**, *5*, 1557−1561.
(16) Mertens, H.; Biteen, J. S.; Atwater, H. A.; Polman, A. Polarization-Selective Plasmon-Enhanced Silicon Quantum-Dot Luminescence. *Nano Lett.* **2006**, *6*, 2622−2625.
(17) Sun, G.; Khurgin, J. B.; Soref, R. A. Practicable Enhancement of Spontaneous Emission Using Surface Plasmons. *Appl. Phys. Lett.* **2007**, *90*, 111107.
(18) DiMaria, J.; Dimakis, E.; Moustakas, T. D.; Paiella, R. Plasmonic Off-Axis Unidirectional Beaming of Quantum-Well Luminescence. *Appl. Phys. Lett.* **2013**, *103*, 251108.
(19) Yu, N.; Genevet, P.; Kats, M. A.; Aieta, F.; Tetienne, J.-P.; Capasso, F.; Gaburro, Z. Light Propagation with Phase Discontinuities: Generalized Laws of Reflection and Refraction. *Science* **2011**, *334*, 333−337.
(20) Ni, X.; Emani, N. K.; Kildishev, A. V.; Boltasseva, A.; Shalaev, V. M. Broadband Light Bending with Plasmonic Nanoantennas. *Science* **2012**, *335*, 427.
(21) Sun, S.; He, Q.; Xiao, S.; Xu, Q.; Li, X.; Zhou, L. Gradient-Index Meta-Surfaces as a Bridge Linking Propagating Waves and Surface Waves. *Nat. Mater.* **2012**, *11*, 426−431.
(22) Sun, S.; Yang, K.-Y.; Wang, C.-M.; Juan, T.-K.; Chen, W. T.; Liao, C. Y.; He, Q.; Xiao, S.; Kung, W.-T.; Guo, G.-Y.; Zhou, L.; Tsai, D. P. High-Efficiency Broadband Anomalous Reflection by Gradient Meta-Surfaces. *Nano Lett.* **2012**, *12*, 6223−6229.
(23) Aieta, F.; Genevet, P.; Kats, M. A.; Yu, N.; Blanchard, R.; Gaburro, Z.; Capasso, F. Aberration-Free Ultrathin Flat Lenses and Axicons at Telecom Wavelengths Based on Plasmonic Metasurfaces. *Nano Lett.* **2012**, *12*, 4932−4936.
(24) Genevet, P.; Yu, N.; Aieta, F.; Lin, J.; Kats, M. A.; Blanchard, R.; Scully, M. O.; Gaburro, Z.; Capasso, F. Ultra-Thin Plasmonic Optical Vortex Plate Based on Phase Discontinuities. *Appl. Phys. Lett.* **2012**, *100*, 013101.
(25) Xu, Y.; Gu, C.; Hou, B.; Lai, Y.; Li, J.; Chen, H. Broadband Asymmetric Waveguiding of Light without Polarization Limitations. *Nat. Commun.* **2013**, *4*, 2561.
(26) Yin, X.; Ye, Z.; Rho, J.; Wang, Y.; Zhang, X. Photonic Spin Hall Effect at Metasurfaces. *Science* **2013**, *339*, 1405−1407.
(27) Karimi, E.; Schulz, S. A.; De Leon, I.; Qassim, H.; Upham, J.; Boyd, R. W. Generating Optical Orbital Angular Momentum at Visible Wavelengths Using a Plasmonic Metasurface. *Light: Sci. Appl.* **2014**, *3*, e167.
(28) Pors, A.; Nielsen, M. G.; Bernardin, T.; Weeber, J.-C.; Bozhevolnyi, S. I. Efficient Unidirectional Polarization-Controlled Excitation of Surface Plasmon Polaritons. *Light: Sci. Appl.* **2014**, *3*, e197.
(29) Lin, D.; Fan, P.; Hasman, E.; Brongersma, M. L. Dielectric Gradient Metasurface Optical Elements. *Science* **2014**, *345*, 298−302.

DOI: 10.1021/acsphotonics.5b00544
ACS Photonics 2016, 3, 243−248